Experimental and theoretical study of photo-dissociation spectroscopy of pyrene dimer radical cations stored in a compact electrostatic ion storage ring

J. Bernard, A. Al-Mogeeth, Serge Martin, G. Montagne, Christine Joblin, L. Dontot, F. Spiegelman, Mathias Rapacioli

Experimental and theoretical study of photo-dissociation spectroscopy of Pyrene dimer radical cations stored in a compact electrostatic ion storage ring

Authors

J. Bernard[1], A. Al-Mogeeth[1], S. Martin[1], G. Montagne[1], C. Joblin[2], L. Dontot[3], F. Spiegelman[3] and M. Rapacioli[3]

[1]Institut Lumière Matière, UMR5306 Université Lyon 1-CNRS, Université de Lyon 69622 Villeurbanne cedex, France

[2]Institut de Recherche en Astrophysique et Planétologie, Université de Toulouse (UPS), CNRS, CNES, 9 Avenue du Colonel Roche, F-31028 Toulouse, France

[3]Laboratoire de Chimie et de Physique Quantiques (LCPQ), IRSAMC, Université de Toulouse (UPS) and CNRS, 118 Route de Narbonne, F-31062 Toulouse, France

Abstract

In this paper, we present an experimental and theoretical study of the photo-dissociation of free-flying dimer radical cations of pyrene $(C_{16}H_{10})_2^+$. Experimentally, the dimers were produced in the plasma of an electron cyclotron resonance ion source and stored in an electrostatic ion storage ring, the Mini-Ring for times up to 10 ms and the photo-dissociation spectrum was recorded in the 400 to 2000 nm range. Two broad absorption bands were observed at 550 (2.25 eV) and 1560 nm (0.79 eV), respectively. Theoretical simulations of the absorption spectrum as a function of the temperature were performed using the Density Functional based Tight Binding approach within the Extended Configuration Interaction scheme (DFTB-EXCI) to determine the electronic structure. The simulation involved all excited electronic states correlated asymptotically with the five lowest excited states D_1-D_5 of the monomer cation and a Monte Carlo exploration of the electronic ground state potential energy surface. The simulations exhibit three major bands at 1.0, 2.1 and 2.8 eV respectively. They allow to assign the experimental band at 1560 nm to absorption by the charge resonance (CR) excited state correlated with the ground state of the monomer D_0. The band at 550 nm is tentatively attributed to dimer states correlated with excited states D_2-D_4, in the monomer cation. Simulations also show that the CR band broadens and shifts towards longer wavelength with increasing temperature. It results from the dependence on the geometry of the energy gap between the ground state and the lowest excited state. The comparison of the experimental spectrum with theoretical spectra at various temperatures allows us to estimate the temperature of the stored $(C_{16}H_{10})_2^+$ in the 300-400 K range, which is also in line with the expected temperatures of the ions deduced from the analysis of the natural decay curve.

Introduction

Polycyclic aromatic hydrocarbons (PAHs) were proposed several decades ago as the emitters of the 3.3, 6.2, 7.7, 8.6 and 11.2 μm bands(1,2), which are commonly observed in several astrophysical environments. Neutral and ionized PAHs are also considered as possible carriers of the diffuse interstellar bands(3). The latter proposition has triggered a variety of studies on gas phase PAHs (4–9) but no individual PAHs could be identified so far as the carrier of specific DIBs. The analysis of astronomical observations have also led to suggest

that PAH clusters are abundant in specific regions(10). However models predict that their lifetime in these environments is short due to thermal evaporation(11,12). Still, it has been noticed that cationic PAH clusters might be more resistant due to an increased bonding energy(13,14). In addition, these species might be involved in the growth of PAHs by photochemistry as suggested by several experiments (15,16).

Investigating the electronic spectroscopy of cationic homo-dimers is thus of interest both for band assignment and for understanding photochemistry. It is well known that small PAHs cationic dimers show mainly two bands(17). The first one, so-called charge resonance (CR) excitation generally labels states correlated with a monomer cation with having a hole in the Highest Occupied Molecular Orbital (HOMO). The second one, so-called local excitation (LE) band corresponds to excitation to dimer states correlated with an excited monomer cation. Actually, the LE states of the dimer obviously also undergo charge resonance together with excitation. Nevertheless, for sake of simplicity, we will keep this imperfect labelling throughout the text. These bands have been recorded in the gas phase for naphthalene dimer radical cations $(C_{14}H_{10})_2^+$ (17–19) but not for dimers involving larger PAH units. The scope of the present work, is to experimentally investigate the photo-dissociation of dimer radical cations of pyrene $(C_{16}H_{10})_2^+$ (pyrene is constituted of four fused benzene rings and is the smallest of the peri-condensed PAHs) via photo-dissociation spectroscopy and to analyze the results with the help of electronic structure calculations and temperature-resolved simulations.

In order to study free-flying $(C_{16}H_{10})_2^+$ ions, we use a home-made (by the Lyon team) electrostatic ion storage, the Mini-Ring(20). In the last decades, electrostatic storage rings and traps have been developed to study many fields. Presently, molecular physics is one of the fields that takes mostly advantages of the properties of these electrostatic storage devices (ESD), such as mass independent storage condition, long observation times (up to hours) due to cryogenic environment available for some of them (21–27). In our previous experimental works, we have been using our compact Mini-Ring, operated at room temperature to study the radiative cooling of PAH cations such as naphthalene, anthracene and pyrene. In all these cases, we have shown that a fast radiative cooling process referred to as recurrent fluorescence (RF), was responsible for the fast reduction of the internal energy of PAH cations produced in the plasma of an electron cyclotron resonance (ECR) ion source(28–31). Recently, the RF photon emission has been directly detected for naphthalene cations using an ion beam trap(32).

From the theoretical side, a few previous studies were concerned with cationic dimers and larger clusters. In particular, Dontot et al. (33,34) introduced a combination of the constrained Density Functional based Tight Binding scheme (DFTB is an approximate DFT scheme) with valence bond Configuration Interaction (DFTB-CI) to investigate specifically cationic complexes. This model has been shown to cure the charge resonance issue(34). It has been used to determine the structural and energetic properties of pyrene cluster cations(33) and turned out to provide a fair agreement with experimental results addressing their thermal evaporation(35), ionization energies(36) and structural properties(37). The equilibrium structure of the $(C_{16}H_{10})_2^+$ ion was found(33) not to be in an eclipsed superimposed parallel D_{2h} arrangement but to present a twist (54 degrees) of the two units around the intermolecular axis, and also a significant dihedral angle between the two molecular planes, resulting in C_1 symmetry. The theoretical dimer dissociation energy in this calculation was found to be 1.07 eV. This value was successfully used as dissociation energy in a model based on Phase Space Theory (PST), which was developed to reproduce the results of collision induced dissociation experiments [42]. A detailed study of the dependence of the electronic spectrum and of its

variation upon geometry fluctuations is certainly a key point in discussing either the absorption or the photo-dissociation spectra at finite temperature.

In the present work, we report data on the relaxation dynamics of stored cationic pyrene dimers up to 10 ms and on their photo-dissociation spectrum. In the theoretical section of the paper, we investigate the photo-absorption spectrum of the pyrene dimer cation and its dependence upon temperature using an extension of the DFTB-CI scheme and Monte Carlo simulations. Finally, we compare the theoretical results with the experimental photo-dissociation data.

Description of the experiment

The experimental setup has been described in details in previous papers(18,28,38). We provide here a brief description of the ECR ion source and the Mini-Ring.

ECR ion sources are plasma devices, which have been widely used in low and high energy accelerator facilities for several decades(39,40). They are able to generate high intensity beams of singly to multiply charged atomic and molecular ions. We were able to produce pyrene ($C_{16}H_{10}$) dimer cations in an ECR ion source by using special tuning conditions: low power (typically in the 0.5-2 W range) of high frequency microwave (HF of 10 GHz) and high pressure (estimated to be in the range of 10^{-2} to 10^{-1} mbar) to generate a plasma as cold as possible, in terms of electronic and ionic temperatures. These temperatures were indirectly controlled by injecting naphthalene ($C_{10}H_8$) vapor as a carrier gas. The pyrene powder was placed in small reservoir drilled in the HF antenna of the source. This reservoir was heated from the outside thanks to the high heat conductivity, at such a temperature that the pyrene powder could be sublimated with an expected constant flow for several days. This temperature was not measured but was controlled by adjusting the power of the heating system. The naphthalene powder was placed in a reservoir connected to the source via a valve with a controllable opening in order to control the pressure in the plasma chamber. During operation, it is expected that the partial pressure of naphthalene was much higher than that of pyrene. The pyrene dimer beam was extracted and accelerated to 12 keV and selected using a 90º selection magnet. It is expected that the formation of the dimer cations is favored by polarization resulting from a long distance attractive force between charged and neutral monomers. A parallel plate deflector biased via a fast electronic switch is used as a chopper to obtain ion bunches of 1 to 5 µs before injection into the Mini-Ring.

The Mini-Ring is composed of four parallel plate deflectors and two electrostatic conical mirrors labelled d_1 to d_4 and c_1-c_2 in the order they are encountered by the ions beam (Figure 1). Details are given in paper(18). The Mini-Ring is equipped with two detectors. A position sensitive detector (PSD) (multichannel plates with a resistive anode) is used to detect neutral fragments resulting from dissociation events between d_3 and d_4 and a channeltron placed behind cone c_1 can be used to detect neutral fragments produced between d_2 and c_1. A Faraday cup (FC) is used as a beam diagnostic after a single turn of ions in the Mini-Ring; therefore, the Mini-Ring can be used as an electrostatic energy analyzer of the beam, which improves the mass resolution.

A 1 kHz repetition rate Nd:YAG laser equipped with an optical parameter oscillator (OPO, EKSPLA model NT242) is used to excite the stored ions. The photo-dissociation spectrum of stored $(C_{16}H_{10})_2^+$ was obtained by scanning the laser wavelength in the visible and near-infrared (IR) range from 400 to 2500 nm and by detecting the subsequent neutral fragments with the PSD. Practically, the laser beam was sent to cross and irradiate the stored $(^{12}C_{16}H_{10})_2^+$

ion beam between d_3 and d_4 at approximately 90° in the same configuration as in ref. (18). The intensity of the laser pulse was in the range of about 30 and 300 μJ/pulse, depending on the wavelength. Corrections of laser power and ion beam intensity fluctuations have been made by recording, simultaneously with the neutral fragments, the laser power and the MCP total counts, which is expected to be proportional to the ion beam intensity.

Experimental results

Figure 2 displays a typical mass spectrum recorded for the production of $(C_{16}H_{10})_2^+$ with optimized source conditions. It was recorded from the ionic current measured at the FC of the Mini-Ring by scanning the selection magnet current. Dominating peaks are from monomers of naphthalene ($C_{10}H_8^+$), pyrene ($C_{16}H_{10}^+$) and anthracene ($C_{14}H_{10}^+$). The presence of anthracene was due to a contamination of the source from previous experiments performed with this molecule. It turned out to be helpful for mass calibration. The dimers of naphthalene, pyrene and anthracene are observed in the high mass range above m/z=250 u. The trimer of naphthalene $(C_{10}H_8)_3^+$ is also present in the mass spectrum at m/z=384 u. In the inset of Figure 2, we observe three peaks at masses corresponding to $(^{12}C_{16}H_{10})_2^+$ and pyrene dimers in which one or two 13C isotopic atoms are incorporated (for pyrene monomer, the abundance of the 13C isotope is 0.17 relative to 1.0 for the main pure 12C isotope). We have checked that the intensity ratios between these three peaks correspond indeed to the natural abundance of ^{13}C. Hence, we exclude the presence of dimers with one or two H atoms loss as observed by Zhen et al.(16) .

The cationic dimers $(^{12}C_{16}H_{10})_2^+$ have been stored for 10 ms in the Mini-Ring in order to record their natural decay. As for naphthalene dimers cations $(C_{10}H_8)_2^+$, the main dissociation process is expected to be the evaporation of a monomer. The natural decay results from dissociation events due to dimer ions containing a high enough internal energy to dissociate in the corresponding time window. In the plasma of the ion source, the temperature is expected to be high enough to induce this natural decay. On the other hand, the plasma temperature is also low enough to lead to the formation of dimers. The natural decay as displayed in Figure 3 shows two contributions: (i) at short time it could be fitted by a $t^{-\alpha}$ power law decay, with $\alpha = 1.06$, attributed to the spontaneous dissociation of the hot $(C_{16}H_{10})_2^+$ and an exponential decay at long times (only partially recorded here) attributed to collisions with the background gas. This approximate t^{-1} power law is typical of a broad internal energy distribution (IED) of the $(C_{16}H_{10})_2^+$ relatively to their dissociation energy(41). In order to constrain the IED, we have simulated decays at fixed internal energies and summed up their contributions with a flat IED (Figure 4a) and, as an example, with an IED presenting a high energy cut-off at 1.4 eV (Figure 4b). In the simulation, the neutral yield resulting from dissociation events at time t is given by the difference of the number of remaining ions at times $t - \frac{\Delta t_{34}}{2}$ and $t + \frac{\Delta t_{34}}{2}$, where $\Delta t_{34}$is the ion flight time between D_3 and D_4, via the following expression:

$$\frac{\Delta N}{N}(t) = e^{-k_D t}\left(e^{k_D\frac{\Delta t_{34}}{2}} - e^{-k_D\frac{\Delta t_{34}}{2}}\right) = 2e^{-k_D t} sinh\left(k_D\frac{\Delta t_{34}}{2}\right)$$

We used microcanonical dissociation rates k_D calculated from the phase space theory evaporation model (Zamith et al. (35)), with a dissociation energy of 1.07 eV following a more recent work by the same authors(42). From this calculation, we derived a power law exponent of -1.13 for an IED including energies up to 1.78 eV, which is in reasonable agreement with the measured value of -1.06 (Figure 4a). This figure also shows that all ions carrying more than about 1.4 eV are dissociated after 1.0 ms of storage, time at which they are

probed with the OPO laser. To further illustrate the point, Figure 4b shows the natural decays that would be obtained if the internal energy distribution had a high-energy cut-off (at half-maximum of 1.4 and 1.5 eV). They would give a decay that would deviate from the power law at times up to about 1 ms and 0.1 ms, respectively. Since, in the experiment, the storage started about 120 µs after the ions were extracted from the source, we conclude that the internal energy distribution had an extension to 1.5 eV at least. Note that the phase space theory evaporation model [35] took into account an average total rotation moment, but the dissociation rates were found to be very poorly sensitive to that factor k_D.

Moreover, it is noteworthy in Figure 4a that the decay of $(C_{16}H_{10})_2^+$ ions of internal energy above 1.45 eV have negligible contributions to the total neutral yield at the time of 1.0 ms at which the laser pulses were fired to perform the photodissociation spectrum. Using the harmonic vibrational modes calculated by Dontot et al. (43) and the Beyer-Swinehart algorithm for harmonic oscillators(44), we can derive from this energy a maximum microcanonical temperature of ~480 K. We do not expect a thermal equilibrium of the ions produced within the plasma source. Therefore, it is difficult to derive a corresponding canonical temperature for the population of ions.

Similarly to $(C_{10}H_8)_2^+$ dimer cations, we did not find evidence for fast radiative cooling for the $(C_{16}H_{10})_2^+$ dimer cations. This cooling process would result in a quenching of the power law causing a faster decrease of the neutral fragment signal compared to the t^{-1} law. This is not observed in Figure 3. This differs from the monomer cations (naphthalene, anthracene and pyrene) for which a fast radiative cooling due to the emission of photons in the visible range attributed to the so-called recurrent fluorescence process (also referred as Poincaré fluorescence) has been observed(28,31,45). Therefore, $(C_{16}H_{10})_2^+$ ions would not radiatively cool by recurrent fluorescence, but only by slow IR emission on larger timescales than those of the present experiments.

Figure 5 shows a zoom-in of a typical record of the neutral counts as a function of the storage time in a time range close to the laser firing time. The choice of shooting the laser pulses after 1.0 ms storage time as in Figure 5 (or after 1.8 ms for the photodissociation spectrum of Figure 6) was guided by the compromise between a considerable reduction of background counts due to the natural decay and keeping a rather high repetition rate of the experiment to reach acceptable statistics for recording the photo-dissociation spectrum on a rather broad wavelength range. Figure 5 was recorded during the wavelength scan of the laser in the 400 nm to 700 nm range, which corresponds to the LE band. It results from the accumulation of 9×10^5 bunches injections in the Mini-Ring. The photodissociation count per injection was about 0.017 on average. Missed double photodissociation events occurring for the same injection can be neglected. We have checked that for the maximum intensity of the OPO output of about 80 mW, two-photon absorption had a negligible effect. It is noteworthy that prompt dissociation only is present in Figure 5 and no delayed laser-induced dissociation could be observed during the turns succeeding laser absorption. This indicates that the populated state of the LE band is dissociative. The same observation, i.e. absence of delayed dissociation, has been made in the 1100 nm to 2000 nm range corresponding to the CR band. Consequently, photon absorption in a CR or LE transition leads to an increase of the energy that would be preferentially transferred to intermolecular modes (see theory results section) and therefore significantly increase the dissociation probability. It is therefore relevant to connect the patterns of the photo-action spectrum to the CR and LE absorption bands

In order to record the photo-dissociation spectrum of Figure 6, a narrow time window around the laser induced dissociation peak has been set, and the counts in this time window

have been recorded as a function of the laser wavelength. As expected, this spectrum shows two broad bands corresponding to the CR and LE bands centered at about 1560 and 550 nm (centroids of the bands), respectively. The observed large bandwidth is expected considering the distribution of internal energies/temperatures associated with the population of probed ions.

Theoretical modeling

The present section is dedicated to the investigation of the electronic structure of the pyrene cation dimer and its photoabsorption spectrum. While qualitative characters in relationship with possible fragmentation of some potential energy surface (PES) are discussed, no explicit fragmentation molecular dynamics is carried out in the present section. As shown in previous studies, a correct account of the electronic structure in relative large cationic molecular systems can be reached using the DFTB-CI scheme. This is briefly summarized hereafter. A set of valence bond type configurations corresponding to a charge localized on a given molecular unit of the cluster is determined from constrained DFTB. This step is followed by a CI within the former generated non-orthogonal basis set. We use in the present work a recent extension (DFTB-EXCI)(46) to compute excited spectra including in the CI not only the configurations with holes in the highest occupied molecular orbitals (HOMOs), but also those in the sub-HOMOs orbitals of each monomer. Moreover, our software has been extended to also include configurations involving virtual orbitals above the HOMO, and in particular the LUMO. Thus, configurations not only correlated with CR states but also with LE states can be generated. In addition, at the difference of our previous work in ref 42, constrained DFTB has been achieved here separately for each excited configuration (rather than using the same Lagrange parameter as for the ground state), which allows a much better localization for the excited states. Note that one advantage of the DFTB-CI or DFTB-EXCI schemes is a correct description of the potential energy surfaces up to dissociation. This is important if one wants to achieve simulations at somewhat high temperature where the system is expected to explore a quite wide area of the PES. The validity of the DFTB-EXCI was assessed in reference [46] against CASPT2 *ab initio* calculations, in particular in concern with the PES behaviour along the elongation and twist pathways. All DFTB calculations have been performed within a locally developed version of the DeMon-Nano code(47).

In the pyrene monomer cation, the symmetry of the D_0 ground state is $^2B_{3g}$. The lowest excited state D_1 with symmetry $^2B_{3g}$ is dipole-forbidden and was theoretically found to lie at 0.85/1.16 eV (48,49), depending on the method. The five lowest dipole-allowed excited electronic states D_2, D_3, D_4, D_5, D_6 with respective symmetries $^2B_{1u}$, ^2A_u, $^2B_{1u}$, ^2A_u, $^2B_{1u}$ were characterized experimentally(50–52) at 1.56/1.58, 1.88/1.74, 2.51/2.55, 2.79 and 3.42 eV respectively (values slightly varying with the authors) and were also investigated theoretically (48,49,53). Almost all states have zero or relatively small oscillator strengths except state D_5, which is strongly absorbing (theoretical oscillator strength of 0.43 or 0.29 in reference (48) depending on the method). These excited states were analyzed in the latter publication (see also Hirata et al.(49) as essentially generated by holes in the HOMO orbitals down to HOMO-4, and also by configurations with an empty HOMO and a single electron in the LUMO (we take here the neutral occupation as the reference). Hence, in the dimer case, we included in the multiconfigurational CI space of the DFTB-EXCI scheme all charge-localized configurations per molecule with holes in HOMO to HOMO-4 plus the configuration with empty HOMO and one electron the LUMO, so that the size of the non-orthogonal CI is 2x6. The present DFTB-EXCI values of the excitation energies of the monomer are 1.01, 1.75, 1.80, 2.34 and 2.51 eV in reasonable agreement with the above values. In the dimer calculation, a first interesting feature, already examined for the lowest states in our previous

publication (46), is the evolution of the excited states features with geometry. In addition, the various valence bond configurations (corresponding to well-defined excitations of the monomers) mix and CI eigenstates, which are asymptotically forbidden, become dipole-allowed at finite intermolecular distance, the detailed features depending on the global symmetry and the specific geometry. We illustrate this dependence by plotting the vertical energy diagram levels in Figure 7 and the spectra in Figure 8, including all presently calculated excited states for two particular dimer geometries, the equilibrium geometry (C_1 symmetry) and the eclipsed (superposed) parallel geometry (D_{2h} symmetry). As expected, the spectrum at the equilibrium geometry has more absorbing components in the region 2-3 eV, due to its lower symmetry *vs* the D_{2h} structure. At equilibrium, the vertical transitions with significant intensities lie at 1.14, 1.73, 2.14, 2.62, 2.66, 2.91, 3.23 and 3.70 eV. Another noticeable feature is the shift of the lower transition energy, corresponding to the antibonding CR state, from 1.15 eV in the C_1 geometry to 0.68 eV in the D_{2h} geometry. One can also note that the ground state of the cation dimer is always essentially spanned by a combination of the CR valence bond components $C_{16}H_{10}^{+}$+$C_{16}H_{10}$ and $C_{16}H_{10}$+$C_{16}H_{10}^{+}$, whatever the geometry. Oppositely, the lowest excited state at the equilibrium structure has a significant weight not only on the antibonding CR component, but also on the higher excited valence bond configurations.

The Monte Carlo simulations of the absorption spectrum using the DFTB-EXCI electronic states and oscillator strengths (from the ground state) were performed with all intermolecular and intramolecular degrees of freedom kept active. The exploration of the electronic ground state PES phase space at finite temperature was achieved via the replica exchange Monte Carlo (MC) (54,55) approach and the DFTB-CI scheme. Replica exchange MC allows geometry switches between parallel walks at different temperatures to increase ergodicity, respecting the canonical ensemble distribution. The exploration consisted of 10 parallel MC runs corresponding to temperatures between 10 and 500 K. Each run is 100000 steps long (single point energy calculations of the electronic ground state), from which 1500 visited structures along the walk (every 60 MC step after an initial thermalization period) are retained for the second stage. The use of DFTB-CI instead of DFTB-EXCI for the global exploration stage of the ground state was chosen for sake of computational efficiency. Indeed the DFTB EXCI method is more time-consuming than the DFTB-CI method, since a larger number of Lagrange constraints must be imposed when more excited electronic configurations are included (this choice is justified by the analysis of the configurational content of the ground state DFTB-EXCI wavefunction for various geometries, see above). We have checked that using DFTB-EXCI instead of DFTB-EXCI does not significantly alter the ground state PES. The second stage consists in the computation of the DFTB-EXCI ground and excited states and the corresponding vertical absorption intensities of the selected structures. The vertical oscillator strengths are accumulated into bins (from 0 to 3 eV with a width of 0.06 eV) to build a synthetic absorption spectrum at a given temperature.

Figure 9 displays the simulated photo-absorption spectra of the pyrene dimer cations at various temperatures between 10 and 500 K. At 10 K, the absorption spectrum of the dimer is characterized by peaks around 1.1, 1.7, 2.1, 2.6, 2.9, 3.2 and 3.7 eV, essentially corresponding to the features at the equilibrium geometry, with the maximum intensity at 2.9 eV. The lowest energy peak at 1.1 eV corresponds to the CR excitation, whereas the highest ones all correspond to local excitation. When the temperature is increased, namely above 200 K, several features characterize the evolution of the spectra: (i) the CR band strongly broadens, covering energies in the range 0.65-1.25 eV; (ii) simultaneously, the CR band center at 1.1 eV at low temperature shifts to the blue by -0.2 eV when the cluster is warmer; (iii) the bands above 1.5 eV tend to merge with increasing temperature, resulting in two broadened bands

around 2.1 and ~2.80 eV. Interestingly, the band at 2.1 eV essentially build up above 200K. The more intense peak also undergoes a temperature shift from 2.9 to 2.8 eV (-0.1eV), significantly smaller than that of the CR band maximum.

Partial insight into the characteristics of the CR absorption band can be obtained through examinations of the potential energy surfaces in reduced dimensionality, constraining the system in parallel configuration as a function of two degrees of freedom, namely the intermolecular separation and the twisting mode only (represented on Figure 10b and 9b', respectively). Maps of the PESs for the ground and first excited CR states are represented in Figure 10c and 9d, respectively. Figure 10 shows the evolution of these two states along selected dissociation (e) and twist cuts (e') (along the dashed horizontal and vertical lines, respectively, in Figure 10c and 9d). The 2D-constrained electronic ground state minimum (is located at the intersection of the two dashed lines). The CR splitting, essentially proportional to the HOMOs overlap, naturally decreases with increasing intermolecular distance (Figure 10e) but also strongly varies according to the twist angle. Figure 10e' shows that the largest splitting values are obtained for twist angles 0 and 54 degrees, the latter corresponding to the most stable structure. At low temperature, one expects the dimer motion to remain close to this geometry, essentially inside the first isocontour around the crossing point of the dashed lines on Figure 10e. The visited region is therefore be associated to large values of the CR splitting and, consequently, to the high-energy contribution of the photo-absorption spectrum. At higher temperature, the system potentially explores a more extended region of the ground state PES limited by the higher energy isocontours of Figure 10c, i.e., mostly visiting regions with increasing intermolecular distances and fluctuating twist angles. Figure 10e and Figure 10e', show that in both cases, this will result in a decrease of the CR splitting and, consequently a broadening of the CR absorption band together with shift toward lower energies. Actually, the MC simulation shows that while the average walk remains confined in the basin of the twisted equilibrium structure for temperatures lowest than 210 K, fluctuation between the former and parallel eclipsed structures (or parallel displaced) do occur above T=300 K. At T=500 K, continuous fluctuations of the twist angle between 0 and 90 degrees is observed, large deviations of the dihedral angle and even the (rare) occurrence of side-bonded structures.

Discussion

Figure 9a shows the temperature evolution of the theoretical absorption spectrum. Although the evolution is small between 210 K and 90 K, the theoretical spectrum at 320 K (Figure 9b) appears to be in best agreement with the experimental photodissociation one (Figure 9c, essentially because of a slight better position of the peak at 2.3 eV). Note that this comparison is meaningful as far as dissociation is fairly direct for all populated states. In the theoretical spectrum, a broad band is associated with the CR absorption with a band center around 1.0 eV (1240 nm). This can be compared with the experimental band, which extends between 1200 and 2000 nm (1.03-0.62 eV) with a maximum around 1530 nm (0.79 eV). The shift of 0.2 eV may be at least partly attributed to the precision of the calculations. The assignment of the experimental LE band at 2.3 eV is more delicate. As previously discussed, it is not expected to result from the dimer states asymptotically correlated with dipole-forbidden state D_1. Actually, there is only a weak and flat contribution in the theoretical spectrum between 1.2 and 1.6 eV. It is also noteworthy that, in the experimental spectrum, the CR and LE bands show an offset between 1.1 and 1.6 eV, where the signal remains small but significantly above zero. The same is observed in the theoretical absorption spectrum. The states above 2 eV are to be assigned to dimer states correlating to monomer asymptotes above D_2. The simulated spectrum at 320 K presents two intense bands in this higher energy region.

The first one centered at 2.1 eV likely derives from monomer states D_2-D_4 and is quite close to the experimental peak. The second band at 2.8 eV with maximal intensity corresponds to states directly correlated or having significant weights on the strongly absorbing monomer state D_5. It is possible that both contributions (at 2.1 and 2.8 eV) predicted by theory are present in the experimental spectrum but mixed within the recorded broad band. The ratio of the maximal intensities that could be attributed to LE bands compared to the CR band is roughly 3 in the experimental spectrum, which appears to be consistent with the peak intensity ratio of the theoretical bands at 2.1 and 1.0 eV. Nevertheless, since the experiment does not provide results above 2.9 eV, it is difficult to ascertain the former assignment with absolute confidence. Despite remaining discrepancies or uncertainties in the comparison between theory and experiment, we conclude that the measured photo-dissociation spectrum is consistent with a population of ions in the range 300-400 K.

Note that we have not discussed the influence of global rotation on dissociation. Fragmentation can obviously be affected in two ways by rotation, namely: (i) classical dynamical effects associated with the centrifugal term result in a usual decrease of the dissociation energy and the presence of a centrifugal barrier; (ii) the possibility of quantum tunneling through the rotational barrier possibly further reduces the apparent dissociation energy threshold. The number of vibrational degrees of freedom in the present system is 150. Thus, at thermal equilibrium, the energy available in the three rotation modes is only a small part of that available to the full system, unlike in small molecules (56). Actually, classical trajectory calculations within PST investigating thermal monomer evaporation from pyrene clusters up to 300 K [42] showed no visible difference between simulations at $J = 0$ and at the most probable J. The isotropic rotational constant of the pyrene dimer at equilibrium is 7.87×10^{-7} eV (structural data obtained from DFTB-CI calculations) and the most probable J for a Boltzman distribution at 300K is $J = 182$ and $J = 235$ at 500 K, which explains the small impact. Considering the small impact of rotation, found with the latter theory, we have not carried out explicit DFTB-CI Molecular Dynamics simulations of fragmentation. The Monte Carlo sampling of the ground state used in the temperature-evolution calculation of the absorption spectrum includes no kinetics. For all the simulated temperatures, no dissociation was observed during the large DFTB-CI/MC sampling. Obviously, description of dissociation in the very vicinity of the threshold is a challenging question, in complex systems like the pyrene dimer cation, in part because of the anisotropic variations of the potential energy surfaces and barrier heights due to intracluster molecular rotational motions and their coupling with vibrational fluctuations. Moreover tunneling effect may be significant. However, their modeling this effect is still today a formidable task for systems with such a large number of degrees of freedom. Quantum investigations of rotation were essentially published for smaller systems, for instance with methods such as wavepacket Multi-Configurational Time-Dependant Hartree method (57) and often in a reduced dimensionality framework or applied to scattering (58,59). Clearly, such a study would be desirable whenever the above techniques will become tractable for systems as large as the pyrene dimer. It would however require a specific and significant effort beyond the scope of the present work.

Bearing in mind that the experiment shows the presence of prompt dissociation, another theoretical advance would be to simulate the full photo-dissociation process beyond the absorption spectrum, which would imply to include non-adiabatic dynamics in the excited states after absorption. This is beyond the scope of the present work. Nevertheless, it can be inferred from the examination of the CR excited state energy levels in Figure 7 that at equilibrium, the vertical transition leads the system above the dissociation energy. This could be different in other geometries in which the CR gap is reduced (for instance in the D_{2h}

symmetry, the excited level lies just below the asymptote). Nevertheless, since in the experiment, the system is supposed to be at rather high temperature, the energy after photon absorption is likely above the dissociation threshold in all cases. The reduced-dimensionality map of the excited CR state in Figure 6 shows that the excitation of a hot dimer in the CR antibonding state is likely to yield easy dissociation, since moreover this antibonding state does not cross any other state on its dissociative pathway. Obviously, only dynamics could provide more insight about driving the absorbed energy into dissociative intermolecular modes or non-dissociative ones (torsion, shear, etc.) or into electronic relaxation. This would also be very helpful to assign more precisely the origin of the experimental LE band discussed just above. A qualitative discussion on the dynamics of photodissociation of the upper states is difficult, since several potential surfaces are involved and numerous avoided crossings are likely to occur among them.

Conclusion

In this work, we have shown that it is possible to form dimer cations of pyrene but also of naphthalene and anthracene in a plasma ion source by cooling the plasma with a rather high pressure of naphthalene. The decay of the pyrene dimer cations, stored in the Mini-Ring, reveals that the dimers dissociate during the experimental timescale, showing that they are relatively hot. We did not find evidence for a significant ion radiative cooling for times up to 10 ms. The experimental photodissociation spectrum shows two broad bands centered at 1560 nm and 550 nm. Simulated photo-absorption spectra were found in reasonable agreement with the experiment, allowing to assign the low energy feature to absorption by a CR state and the highest energy more intense one to LE states correlating to cation monomer states above D_2. More detailed discussion of the experimental photoactive states in this region is difficult due to the large number of involved states. Analysis of theoretical spectra at various temperatures shows that the position and width of the CR band is especially sensitive to the temperature. This is consistent with previous observations in the case of naphthalene dimer cations from comparison of experiments at high temperature(18) and at low temperature in a supersonic Ar gas jet(17). By comparing the simulated CR band with the measured one, we conclude that the studied dimer cations of pyrene have internal temperatures in the 300-400 K range. From the dynamics of photo-dissociation and the results of calculations on the electronic structure, we can conclude that some direct dissociation pathways following photon absorption exist in the CR and first LE band.

This work provides new data to quantify the lifetime of PAH dimer cations in astrophysical environments. In particular, the presence of direct dissociation channels at low energies implies that other pathways (e.g., thermal dissociation, radiative cooling) cannot significantly contribute to energy relaxation. This will be a strong limitation in the survival of these species in the photon-irradiated regions where these species are possibly present. On the laboratory side, the availability of cryogenic ion storage ring opens the possibility to record the photo-dissociation spectrum in a wide storage time range up to several seconds at which the dimer ions are expected to be colder due to IR emission(60). On the theoretical side, the present study illustrates the possibility for the DFTB-derived scheme, DFTB-EXCI, to account for the electronic spectroscopy of cationic molecular clusters when relatively large molecules and high electronic states are involved, despite the inherent approximations of the method. The present work has combined MC simulations with DFTB-CI to provide sampling at finite temperature. Molecular dynamics including total rotation contribution to explicitly simulate ground state fragmentation has not yet been performed. Theoretical investigation of tunneling at threshold for such a large system remains a challenge. In addition, definite assignment of the photo-dissociation spectrum and theoretical insight in the time evolution of photo-

dissociation will require non-adiabatic molecular dynamics investigation of the relaxation processes in complement to the absorption spectrum.

ACKNOWLEDGMENTS

We acknowledge Sébastien Zamith for providing us the dissociative rates used in the modeling of the natural decay. This work was funded by Agence Nationale pour la Recherche, grant: ANR Program No. ANR-10-BLAN-0426 “Anneau”, the European Research Council under the European Union’s Seventh Framework Program (FP/2007-2013) ERC-2013-SyG, Grant agreement N° 610256 NANOCOSMOS and CNRS GDR3553 EMIE. Simulations were achieved on the CALMIP Meso Center computing platform (project 1743).

FIGURES AND FIGURE CAPTIONS

Figure 1: Schematics of the Mini-Ring

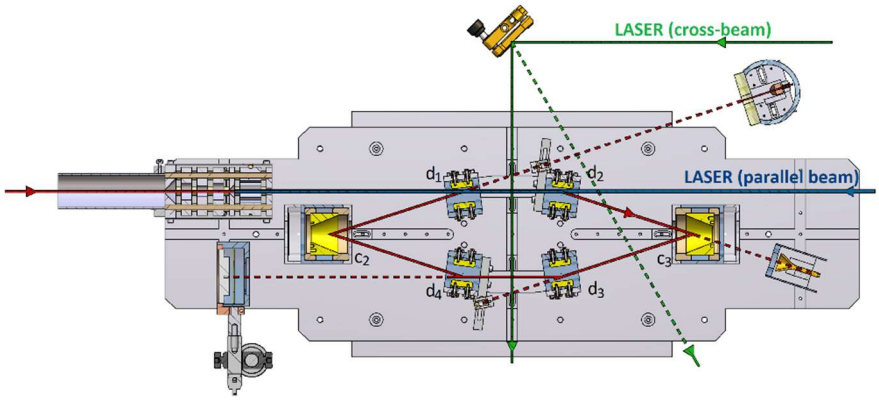

Figure 2: Mass spectrum recorded from the ionic current measured at the Faraday cup (FC) of the Mini-Ring. A mixture of naphthalene and pyrene was injected in the ion source. The presence of anthracene cations ($C_{14}H_{10}^{+}$) resulted from contamination from previous experiments performed with this molecule. We note on the high mass side the presence of naphthalene dimers and trimers, anthracene dimers in very small amounts, and pyrene dimers. Typical ionic current for the $(C_{16}H_{10})_2^{+}$ peak was measured in the range of 10 pA. By the way, we remark tiny peaks at about 306 and 330 amu that can be attributed to naphthalene-anthracene and naphthalene-pyrene hetero-dimers, respectively.

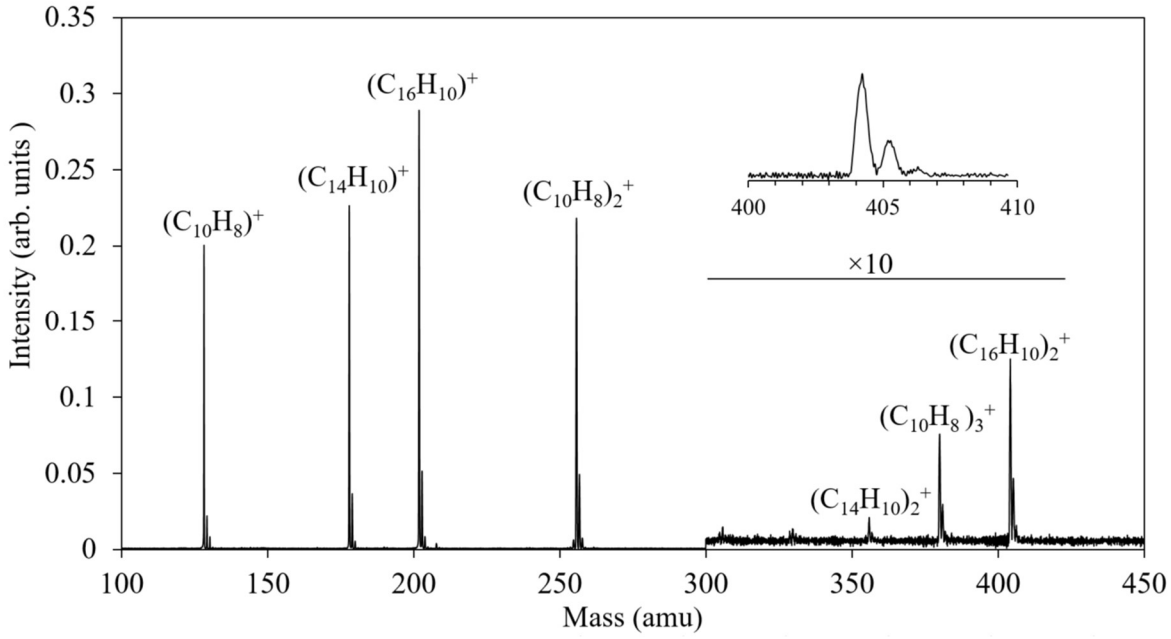

Figure 3: Natural decay of dimer pyrene cations (black dots). The red plain line is a power law best fit the natural decay at short times ($t^{-1.06}$ was found). The deviation of the power law at longer time is attributed to enhanced neutral fragment yield due to collisions of stored $(C_{16}H_{10})_2^+$ with background gas (detector background counts are negligible here). The blue dashed line is the $t^{-1.13}$ power law found in the simulations.

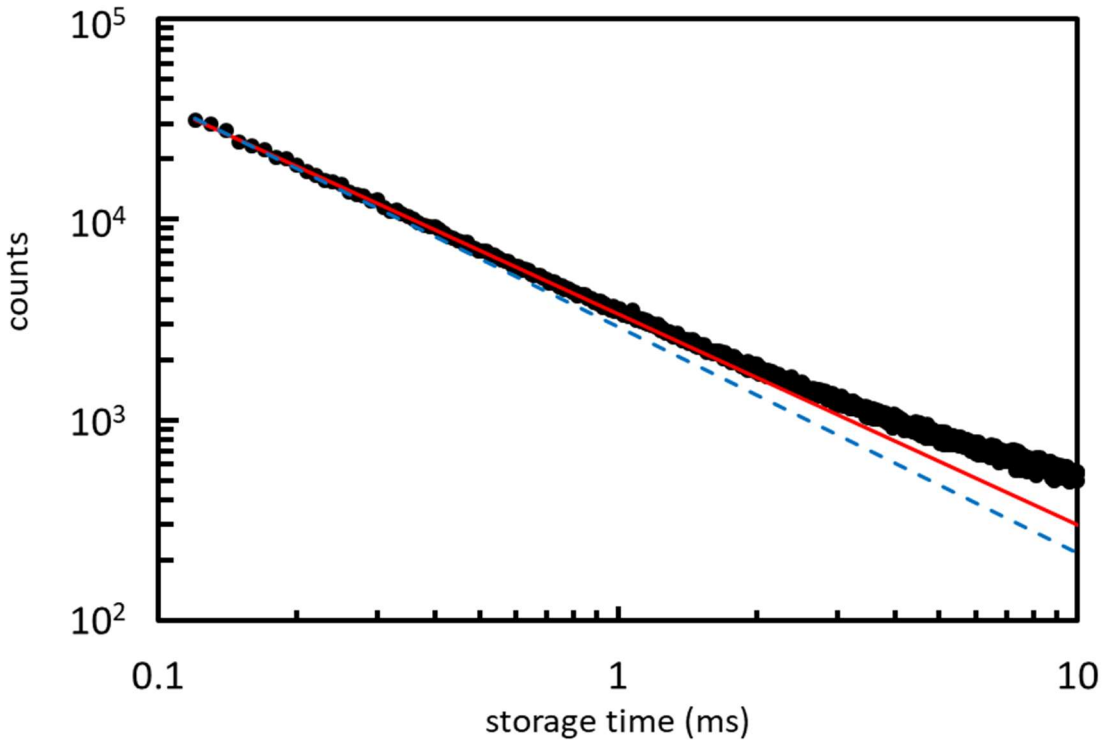

Figure 4: (a) Simulated natural decays (black plain line) assuming a flat (infinitely broad) internal energy distribution computed by summing the contributions of decays at specific internal energies E (few examples amongst the 131 energies that were included in the calculation are displayed here). $t^{-1.06}$ (dotted line) and $t^{-1.13}$ (dashed lines) power laws are also displayed for comparison. (b) Same as (a), assuming a cut-off at 1.4 eV (dash-dotted line) and at 1.5 eV (plain line). The displayed individual energy contributions are those for a cut-off at 1.4 eV. The three different internal energy distributions are plotted in (c) (dashed line: flat IED; plain line: IED with high energy cut-off at 1.5 eV at half-maximum; dash-dotted line: IED with high energy cut-off at 1.5 eV at half-maximum).

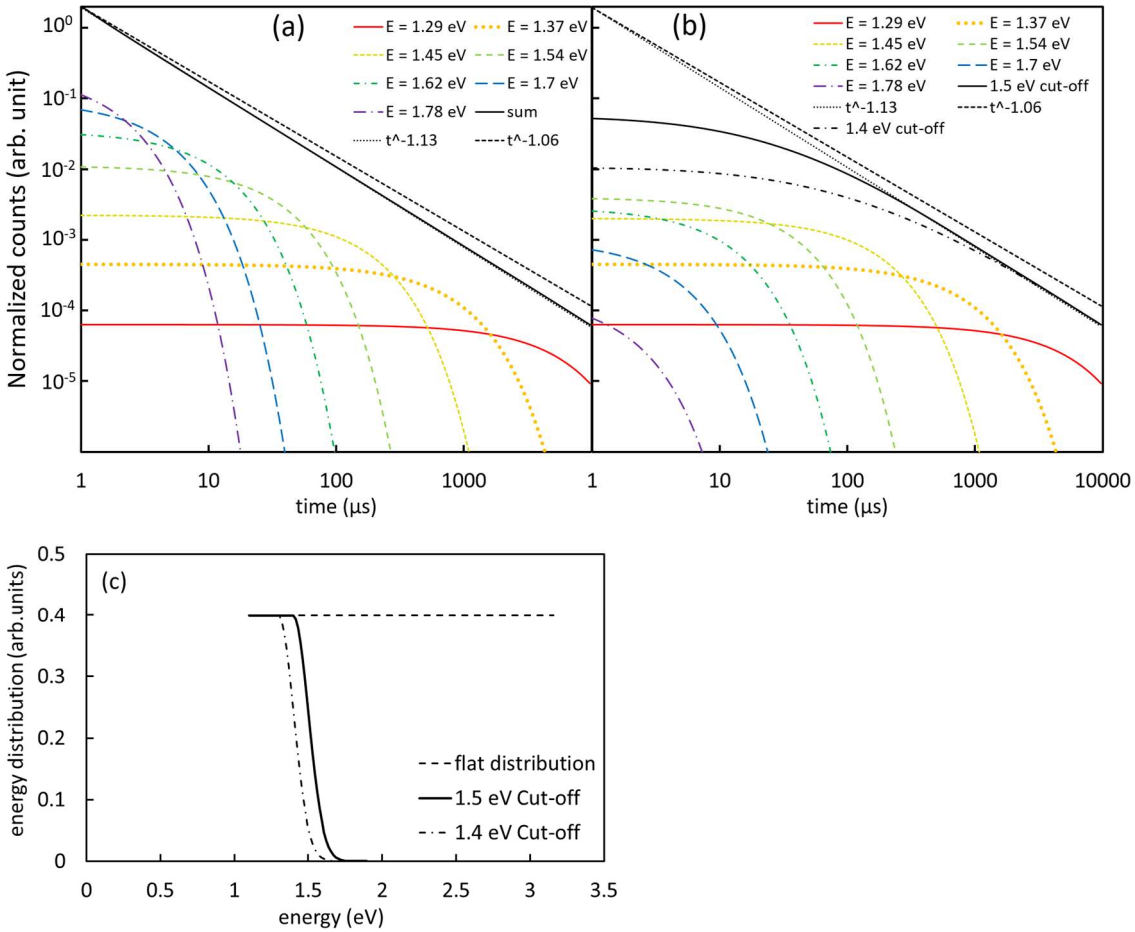

Figure 5: Typical integrated neutral fragment counts recorded at storage times of about 1 ms during a wavelength scan of the laser in the range 400 to 700 nm (LE band). This graph results from the accumulation of 9×10^5 injections. The photodissociation count per injection was about 0.017 on average. The sharp peak is due to laser-induced dissociation. The plateaus are due to the summed counts resulting from the natural decay and from the dissociation induced by collisions with background gas. The absence of delayed laser-induced dissociation is noteworthy.

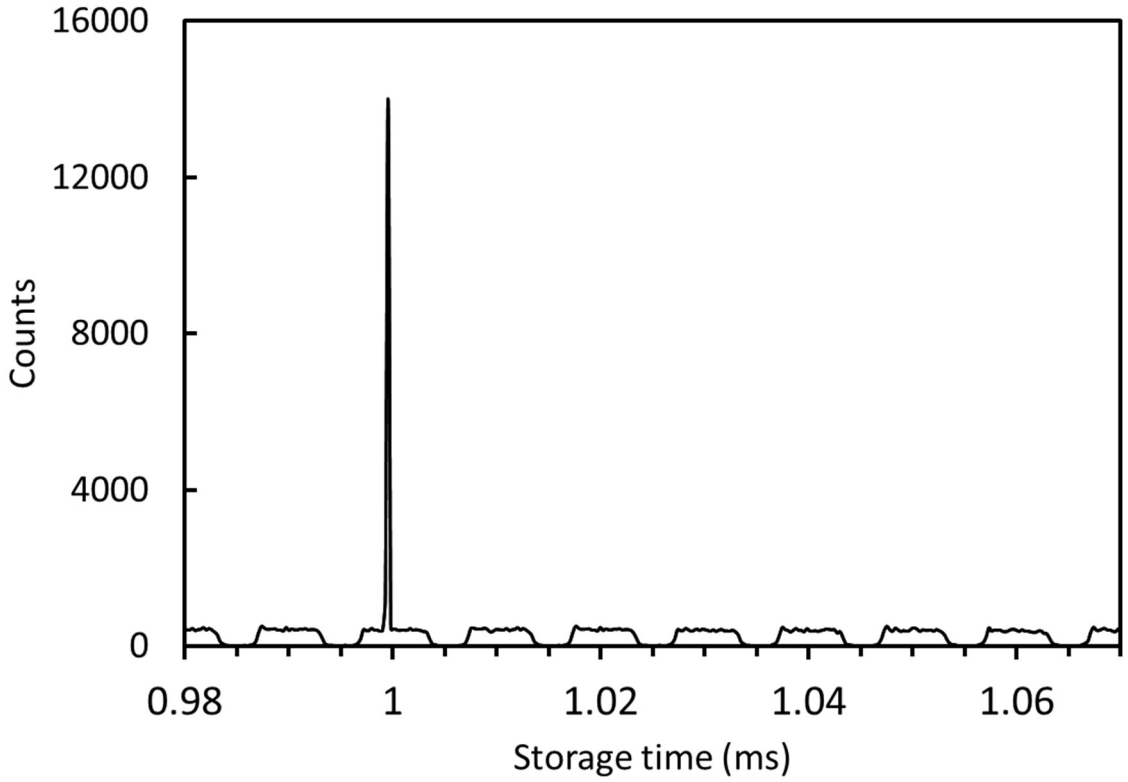

Figure 6: Photo-dissociation (or action) spectrum of $(C_{16}H_{10})_2^+$. Raw data have been corrected for laser intensity variation as a function of wavelength and ion beam fluctuations. Background signal due to collisions with background gas has also been subtracted.

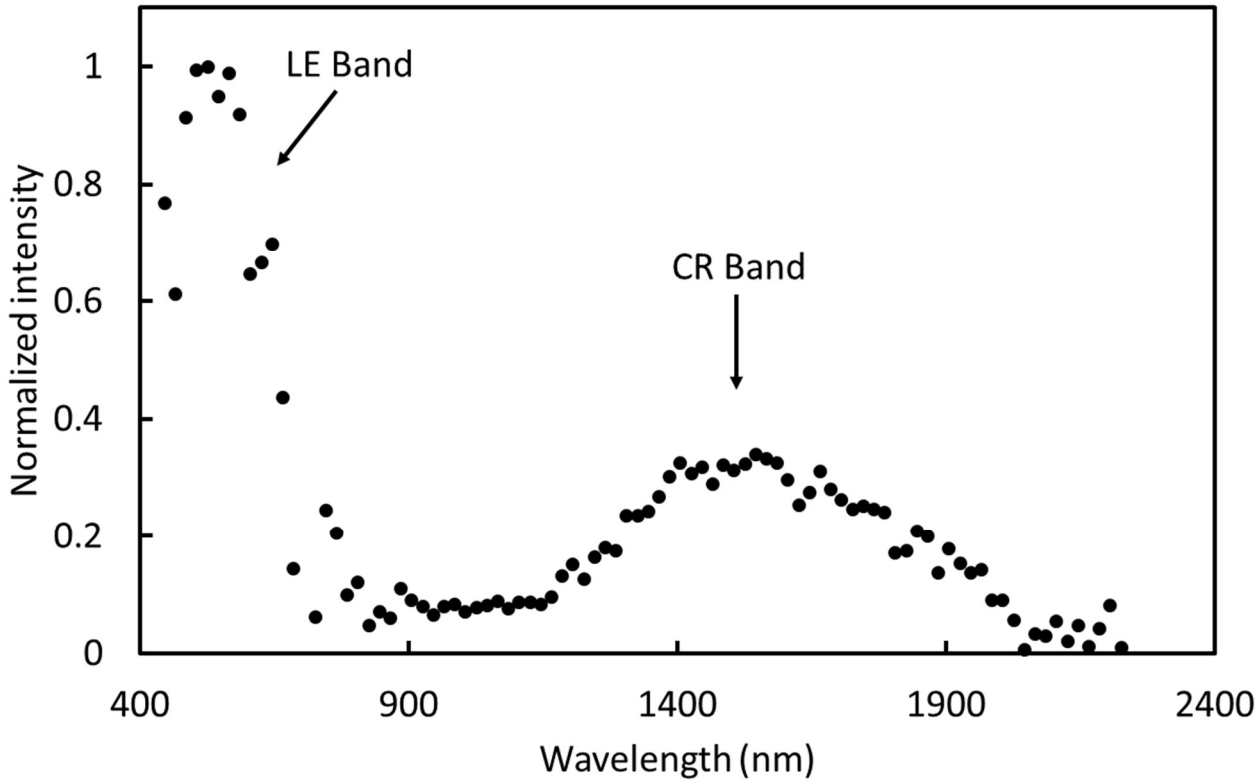

Figure 7: Energy level diagram for three geometric configurations of the pyrene dimer cation (left: energy levels at infinite separation, center: energy levels for the D_{2h}-constrained minimum, at intermolecular distance R=2.98 Å; right: energy levels at the equilibrium geometry). The reference energy corresponds to the ground state of $(C_{16}H_{10})_2^+ + (C_{16}H_{10})_2$ at dissociation. The blue line shows the correlation of the CR bonding and antibonding states.

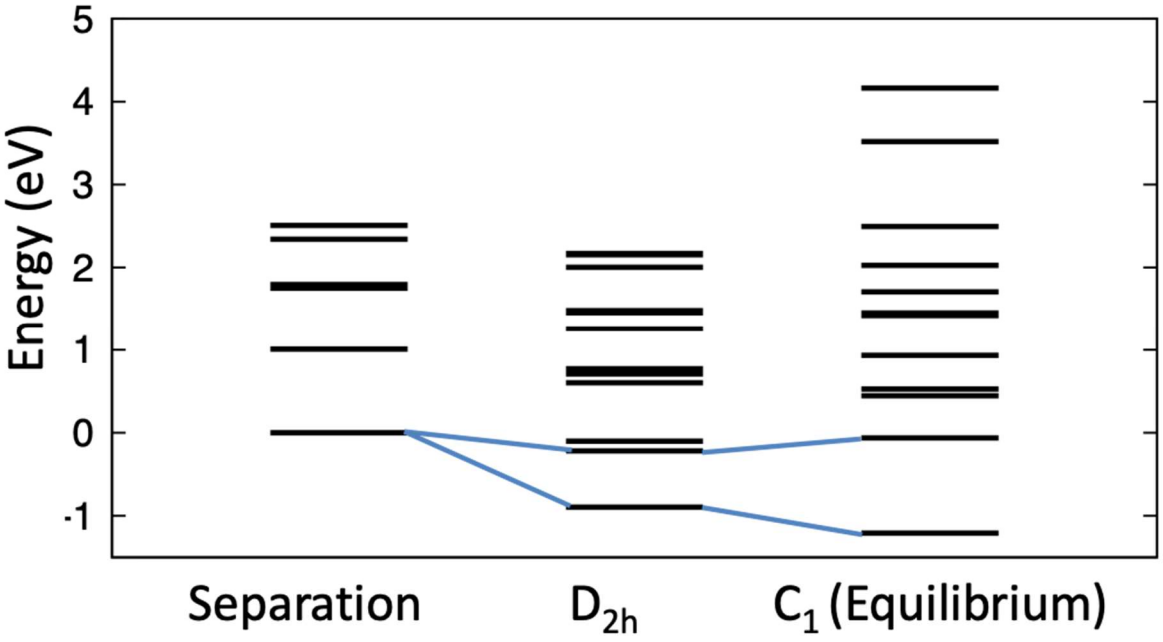

Figure 8: Vertical absorption spectra for two geometric configurations of the pyrene dimer cation: D_{2h} - constrained minimum at R=2.98 Å (a) and equilibrium geometry (b). The symbols indicate state positions while sticks provide intensities.

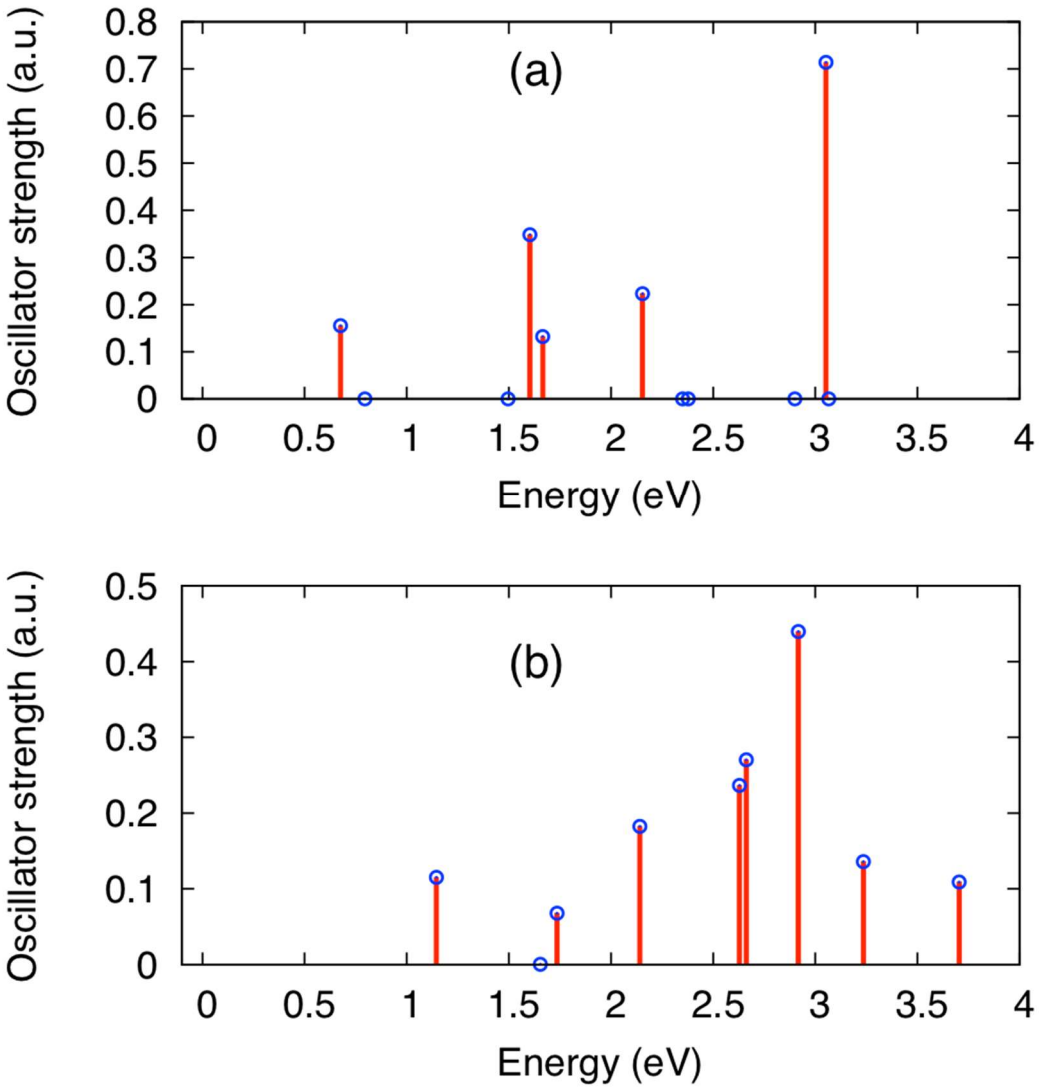

Figure 9: Total absorption spectrum of the pyrene dimer cation $(C_{16}H_{10})_2^+$. Left: Monte Carlo simulation of the temperature evolution between 10 K and 500 K. Right: comparison of the simulated spectrum at 320 K and of the experimental spectrum (normalized at the experimental maximum at 2.3 eV)

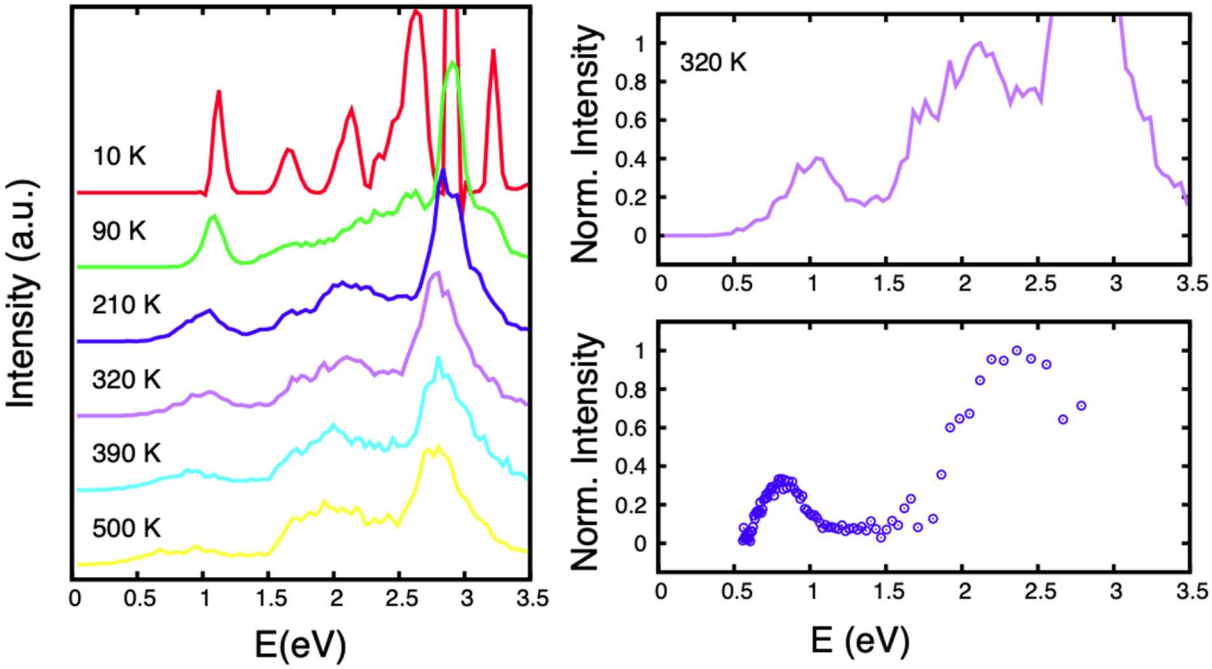

Figure 10 : (a) Equilibrium structure of the pyrene dimer cation ((33), without freezing any degree of freedom); (b, b') Definition of the intermolecular distance and twist angle in sandwich structures (molecular planes parallel); PES reduced to the two aforementioned dimensions for the ground (c) and first excited (d) states, involved in the CR transition. Cuts of these surfaces along a dissociation at 54°(e) and twist mode at 2.98 Å (e').

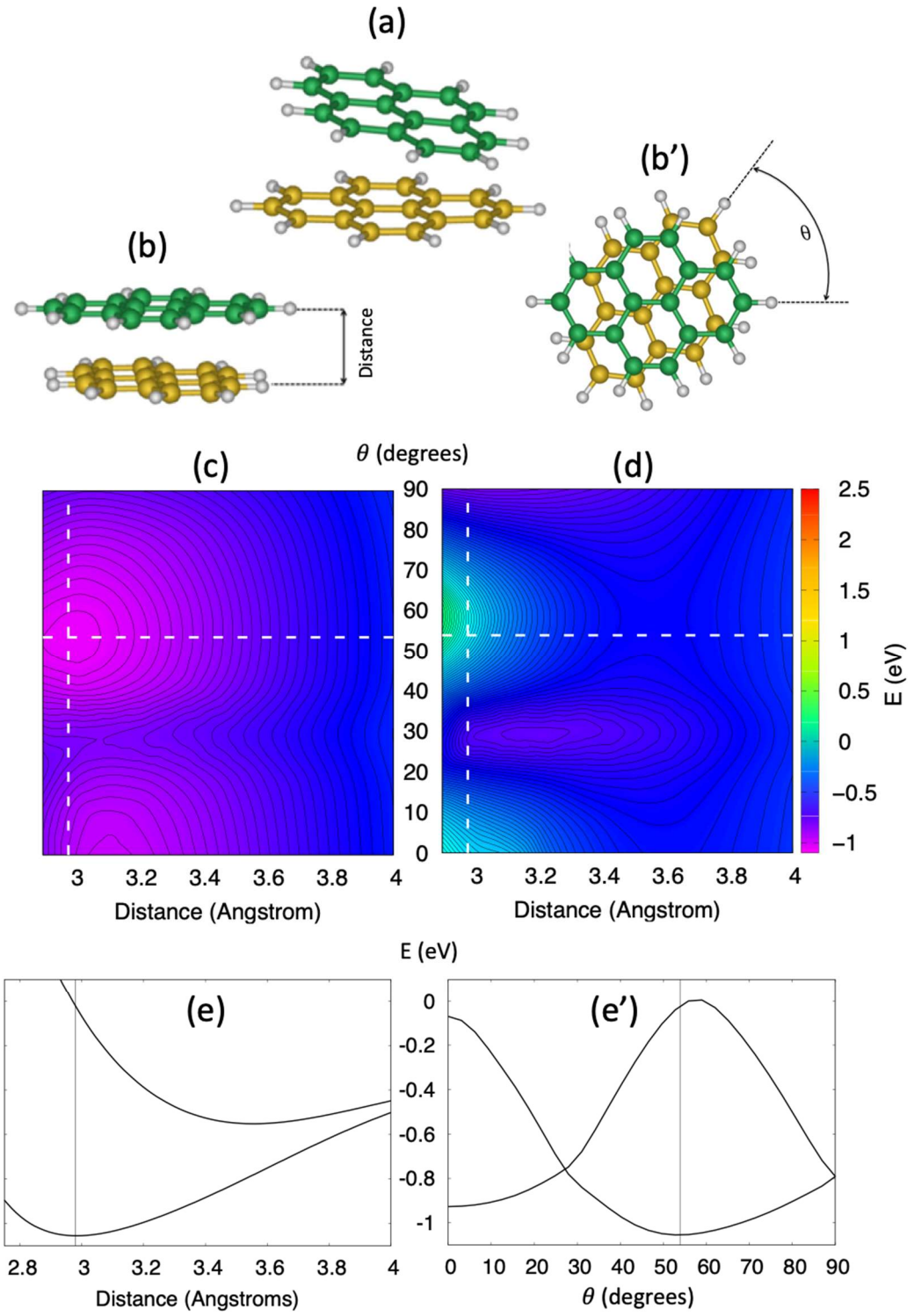

REFERENCES

1. Leger A, Puget JL. Identification of the « unidentified » IR emission features of interstellar dust? Astron Astrophys. 1 août 1984;137:L5-8.

2. Allamandola LJ, Tielens AGGM, Barker JR. Polycyclic aromatic hydrocarbons and the unidentified infrared emission bands - Auto exhaust along the Milky Way. Astrophys J. mars 1985;290:L25-8.

3. Salama F, Galazutdinov GA, Krełowski J, Allamandola LJ, Musaev FA. Polycyclic Aromatic Hydrocarbons and the Diffuse Interstellar Bands: A Survey. Astrophys J. 20 nov 1999;526(1):265.

4. Sukhorukov O, Staicu A, Diegel E, Rouillé G, Henning Th, Huisken F. D2 ← D0 transition of the anthracene cation observed by cavity ring-down absorption spectroscopy in a supersonic jet. Chem Phys Lett. 11 mars 2004;386(4–6):259-64.

5. Tan X, Salama F. Cavity ring-down spectroscopy of jet-cooled 1-pyrenecarboxyaldehyde (C17H10O) and 1-methylpyrene (C17H12) cations. Chem Phys Lett. 10 mai 2006;422(4):518-21.

6. Rouillé G, Arold M, Staicu A, Krasnokutski S, Huisken F, Henning Th, et al. S1(A11)←S0(A11) transition of benzo[g,h,i]perylene in supersonic jets and rare gas matrices. J Chem Phys. 7 mai 2007;126(17):174311.

7. Kokkin DL, Troy TP, Nakajima M, Nauta K, Varberg TD, Metha GF, et al. The Optical Spectrum of a Large Isolated Polycyclic Aromatic Hydrocarbon: Hexa- peri - hexabenzocoronene, C 42 H 18. Astrophys J. juin 2008;681(1):L49–L51.

8. Useli-Bacchitta F, Bonnamy A, Mulas G, Malloci G, Toublanc D, Joblin C. Visible photodissociation spectroscopy of PAH cations and derivatives in the PIRENEA experiment. Chem Phys. 25 mai 2010;371(1):16-23.

9. Salama F, Galazutdinov G, Krelowski J, Biennier L, Beletsky Y, Song I. PAHs in Translucent Interstellar Clouds. 1 mai 2011;218:129.16.

10. Rapacioli M, Joblin C, Boissel P. Spectroscopy of polycyclic aromatic hydrocarbons and very small grains in photodissociation regions. Astron Astrophys. 1 janv 2005;429(1):193-204.

11. Rapacioli M, Calvo F, Joblin C, Parneix P, Toublanc D, Spiegelman F. Formation and destruction of polycyclic aromatic hydrocarbon clusters in the interstellar medium. Astron Astrophys. 1 déc 2006;460(2):519-31.

12. Montillaud J, Joblin C. Absolute evaporation rates of non-rotating neutral polycyclic aromatic hydrocarbon clusters. Astron Astrophys. juill 2014;567:A45.

13. Rhee YM, Lee TJ, Gudipati MS, Allamandola LJ, Head-Gordon M. Charged polycyclic aromatic hydrocarbon clusters and the galactic extended red emission. Proc Natl Acad Sci. 27 mars 2007;104(13):5274-8.

14. Rapacioli M, Spiegelman F. Modelling singly ionized coronene clusters. Eur Phys J D. 1 avr 2009;52(1):55-8.

15. Gatchell M, Delaunay R, Maclot S, Chen T, Stockett MH, Domaracka A, et al. Ion-Induced Reactivity in Pyrene Clusters. J Phys Conf Ser. 29 janv 2015;583:012011.

16. Zhen J, Chen T, Tielens AGGM. Laboratory Photochemistry of Pyrene Clusters: An Efficient Way to Form Large PAHs. Astrophys J. 17 août 2018;863(2):128.

17. Inokuchi Y, Ohashi K, Matsumoto M, Nishi N. Photodissociation Spectrum of Naphthalene Dimer Cation. J Phys Chem. 1 mars 1995;99(11):3416-8.

18. Bernard J, Al-Mogeeth A, Allouche A-R, Chen L, Montagne G, Martin S. Photo-dissociation of naphthalene dimer cations stored in a compact electrostatic ion storage ring. J Chem Phys. 7 févr 2019;150(5):054303.

19. Fujiwara T, Lim EC. Binding Energies of the Neutral and Ionic Clusters of Naphthalene in Their Ground Electronic States. J Phys Chem A. 1 juin 2003;107(22):4381-6.

20. Bernard J, Montagne G, Brédy R, Terpend-Ordacière B, Bourgey A, Kerleroux M, et al. A « tabletop » electrostatic ion storage ring: Mini-Ring. Rev Sci Instrum. 1 août 2008;79:075109.

21. Schmidt HT, Thomas RD, Gatchell M, Rosén S, Reinhed P, Löfgren P, et al. First storage of ion beams in the Double Electrostatic Ion-Ring Experiment: DESIREE. Rev Sci Instrum. 1 mai 2013;84:055115-055115-6.

22. Chandrasekaran V, Kafle B, Prabhakaran A, Heber O, Rappaport M, Rubinstein H, et al. Determination of Absolute Recurrent Fluorescence Rate Coefficients for C6–. J Phys Chem Lett. 4 déc 2014;5(23):4078-82.

23. Ito G, Furukawa T, Tanuma H, Matsumoto J, Shiromaru H, Majima T, et al. Cooling Dynamics of Photoexcited C6- and C6H-. Phys Rev Lett. 1 mai 2014;112:183001.

24. Møller SP. ELISA - An Electrostatic Storage Ring for Atomic Physics. :3.

25. Zajfman D, Heber O, Vejby-Christensen L, Ben-Itzhak I, Rappaport M, Fishman R, et al. Electrostatic bottle for long-time storage of fast ion beams. Phys Rev A. 1 mars 1997;55(3):R1577-80.

26. von Hahn R, Becker A, Berg F, Blaum K, Breitenfeldt C, Fadil H, et al. The cryogenic storage ring CSR. Rev Sci Instrum. 1 juin 2016;87(6):063115.

27. Doussineau T, Antoine R, Santacreu M, Dugourd P. Pushing the Limit of Infrared Multiphoton Dissociation to Megadalton-Size DNA Ions. J Phys Chem Lett. 16 août 2012;3(16):2141-5.

28. Martin S, Bernard J, Brédy R, Concina B, Joblin C, Ji M, et al. Fast Radiative Cooling of Anthracene Observed in a Compact Electrostatic Storage Ring. Phys Rev Lett [Internet]. 7 févr 2013 [cité 29 janv 2019];110(6). Disponible sur: https://link.aps.org/doi/10.1103/PhysRevLett.110.063003

29. Ortega C, Kono N, Ji M, Bredy R, Bernard J, Joblin C, et al. Dissociation rate, fluorescence and Infrared radiative cooling rates of Naphthalene studied in electrostatic storage Miniring. In: Diaz C, Rabadan I, Garcia G, Mendez L, Martin F, éditeurs. Xxix International Conference on Photonic, Electronic, and Atomic Collisions (icpeac2015), Pts 1-12. Bristol: Iop Publishing Ltd; 2015. p. 032051.

30. Ji M, Bernard J, Chen L, Brédy R, Ortéga C, Joblin C, et al. Cooling of isolated anthracene cations probed with photons of different wavelengths in the Mini-Ring. J Chem Phys. 28 janv 2017;146(4):044301.

31. Bernard J, Chen L, Brédy R, Ji M, Ortéga C, Matsumoto J, et al. Cooling of PAH cations studied with an electrostatic storage ring. Nucl Instrum Methods Phys Res Sect B Beam Interact Mater At. 1 oct 2017;408:21-6.

32. Saito M, Kubota H, Yamasa K, Suzuki K, Majima T, Tsuchida H. Direct measurement of recurrent fluorescence emission from naphthalene ions. Phys Rev A. 28 juill 2020;102(1):012820.

33. Dontot L, Spiegelman F, Rapacioli M. Structures and Energetics of Neutral and Cationic Pyrene Clusters. J Phys Chem A. 7 nov 2019;123(44):9531-43.

34. Rapacioli M, Spiegelman F, Scemama A, Mirtschink A. Modeling Charge Resonance in Cationic Molecular Clusters: Combining DFT-Tight Binding with Configuration Interaction. J Chem Theory Comput. 11 janv 2011;7(1):44-55.

35. Zamith S, Ji M-C, L'Hermite J-M, Joblin C, Dontot L, Rapacioli M, et al. Thermal evaporation of pyrene clusters. J Chem Phys. 21 nov 2019;151(19):194303.

36. Joblin C, Dontot L, Garcia GA, Spiegelman F, Rapacioli M, Nahon L, et al. Size Effect in the Ionization Energy of PAH Clusters. J Phys Chem Lett. 3 août 2017;8(15):3697-702.

37. Lei L, Yao Y, Zhang J, Tronrud D, Kong W, Zhang C, et al. Electron Diffraction of Pyrene Nanoclusters Embedded in Superfluid Helium Droplets. J Phys Chem Lett. 6 févr 2020;11(3):724-9.

38. Bernard J, Montagne G, Brédy R, Terpend-Ordacière B, Bourgey A, Kerleroux M, et al. A « tabletop » electrostatic ion storage ring: Mini-Ring. Rev Sci Instrum. 1 août 2008;79:075109.

39. Geller R. Electron Cyclotron Resonance Ion Sources and ECR Plasmas. CRC Press; 1996. 456 p.

40. Geller R. ECRIS: The Electron Cyclotron Resonance Ion Sources. Annu Rev Nucl Part Sci. 1990;40(1):15-44.

41. Hansen K, Andersen JU, Hvelplund P, Møller SP, Pedersen UV, Petrunin VV. Observation of a 1/t Decay Law for Hot Clusters and Molecules in a Storage Ring. Phys Rev Lett. 29 août 2001;87(12):123401.

42. Zamith S, L'Hermite J-M, Dontot L, Zheng L, Rapacioli M, Spiegelman F, et al. Threshold collision induced dissociation of pyrene cluster cations. J Chem Phys. 7 août 2020;153(5):054311.

43. Léo Dontot, Fernand Spiegelman, Sébastien Zamith, Mathias Rapacioli. Dependence upon charge of the vibrational spectra of small Polycyclic Aromatic Hydrocarbon clusters : the example of pyrene. European Physical Journal D. in Press;

44. Stein SE, Rabinovitch BS. Accurate evaluation of internal energy level sums and densities including anharmonic oscillators and hindered rotors. J Chem Phys. 15 mars 1973;58(6):2438-45.

45. Martin S, Ji M, Bernard J, Brédy R, Concina B, Allouche AR, et al. Fast radiative cooling of anthracene: Dependence on internal energy. Phys Rev A. 25 nov 2015;92(5):053425.

46. Dontot L, Suaud N, Rapacioli M, Spiegelman F. An extended DFTB-CI model for charge-transfer excited states in cationic molecular clusters: model studies versus ab initio calculations in small PAH clusters. Phys Chem Chem Phys. 2016;18(5):3545-57.

47. Heine T, Rapacioli M, Patchkovskii S, Frenzel J, Koster A, Calaminici P, et al. deMonNano, [Internet]. 2009; Disponible sur: http://demon-nano.ups-tlse.fr/

48. Negri F, Zgierski MZ. On the vibronic structure of the absorption spectra of radical cations of some polycyclic aromatic hydrocarbons. J Chem Phys. 15 janv 1994;100(2):1387-99.

49. Hirata S, Head-Gordon M, Szczepanski J, Vala M. Time-Dependent Density Functional Study of the Electronic Excited States of Polycyclic Aromatic Hydrocarbon Radical Ions. J Phys Chem A. 1 juin 2003;107(24):4940-51.

50. Khan ZH. Electronic spectra of radical cations and their correlation with photoelectron spectra—V. Pyrenes. Spectrochim Acta Part Mol Spectrosc. 1 janv 1989;45(2):253-70.

51. Szczepanski J, Vala M, Talbi D, Parisel O, Ellinger Y. Electronic and Vibrational-Spectra of Matrix-Isolated Anthracene Radical Cations - Experimental and Theoretical Aspects. J Chem Phys. 15 mars 1993;98(6):4494-511.

52. Salama F, Joblin C, Allamandola LJ. Neutral and ionized PAHs: contribution to the interstellar extinction. Planet Space Sci. 1 oct 1995;43(10):1165-73.

53. Vala M, Szczepanski J, Pauzat F, Parisel O, Talbi D, Ellinger Y. Electronic and Vibrational Spectra Of Matrix-Isolated Pyrene Radical Cations: Theoretical and Experimental Aspects. J Phys Chem. 1 sept 1994;98(37):9187-96.

54. Swendsen RH, Wang J-S. Replica Monte Carlo Simulation of Spin-Glasses. Phys Rev Lett. 24 nov 1986;57(21):2607-9.

55. Calvo F. All-exchanges parallel tempering. J Chem Phys. 22 sept 2005;123(12):124106.

56. Anderson EK, Schmidt-May AF, Najeeb PK, Eklund G, Chartkunchand KC, Rosen S, et al. Spontaneous Electron Emission from Hot Silver Dimer Anions: Breakdown of the Born-Oppenheimer Approximation. Phys Rev Lett. 2020;5.

57. Meyer H-D. Studying molecular quantum dynamics with the multiconfiguration time-dependent Hartree method. WIREs Comput Mol Sci. 2012;2(2):351-74.

58. Milot R, Jansen APJ. Ten-dimensional wave packet simulations of methane scattering. J Chem Phys. 21 juill 1998;109(5):1966-75.

59. Füchsel G, Thomas PS, Uyl J den, Öztürk Y, Nattino F, Meyer H-D, et al. Rotational effects on the dissociation dynamics of CHD3 on Pt(111). Phys Chem Chem Phys. 9 mars 2016;18(11):8174-85.

60. Stockett MH, Björkhage M, Cederquist H, Schmidt HT, Zettergren H. Storage time dependent photodissociation action spectroscopy of polycyclic aromatic hydrocarbon cations in the cryogenic electrostatic storage ring DESIREE. Faraday Discuss. 18 juill 2019;217(0):126-37.